

Terahertz lasers based on germanium and silicon

To cite this article: H-W Hübers *et al* 2005 *Semicond. Sci. Technol.* **20** S211

View the [article online](#) for updates and enhancements.

Related content

- [Nonequilibrium electron distribution in terahertz intracentre silicon lasers](#)
S G Pavlov, H-W Hübers, E E Orlova *et al.*
- [Electrons and optic phonons in solids-the effects of longitudinal optical lattice vibrations on the electronic excitations of solids](#)
P G Harper, J W Hodby and R A Stradling
- [Stimulated emission on impurity – band optical transitions in semiconductors](#)
N A Bekin and V N Shastin

Recent citations

- [Benjamin S. Williams and Qing Hu](#)
- [Roger Lewis](#)
- [Dynamics of a single-atom electron pump](#)
J. van der Heijden *et al*

Terahertz lasers based on germanium and silicon

H-W Hübers¹, S G Pavlov¹ and V N Shastin²

¹ German Aerospace Center (DLR), Institute of Planetary Research, Rutherfordstrasse 2, 12489 Berlin, Germany

² Institute for Physics of Microstructures, Russian Academy of Sciences, GSP-105, 603950 Nizhny Novgorod, Russia

Received 30 March 2005

Published 8 June 2005

Online at stacks.iop.org/SST/20/S211

Abstract

Recent experimental and theoretical results of impurity doped germanium and silicon terahertz lasers are reviewed. Three different laser mechanisms exist in p-type germanium. Depending on the operating conditions and the properties of the crystal, laser transitions can occur between light- and heavy-hole subbands, between particular light-hole Landau levels or between impurity states. Electric and magnetic fields are required for laser operation. In n-type silicon lasing originates solely from impurity transitions of group-V donors, which are optically excited. The properties of these lasers depend upon the chemical nature of the impurity centre and the properties of the host material. The principles of operation are discussed in terms of their basic physical concepts. The state-of-the-art performance of these lasers is summarized.

1. Introduction

A wealth of phenomena has characteristic signatures that fall into the terahertz (THz) part of the electromagnetic spectrum. Among them are the energy gap of superconductors, energy levels of impurities in semiconductors, cyclotron resonance and lattice vibrations in solids and rotational spectra of molecules [1, 2]. Correspondingly there are many applications ranging from remote sensing of astronomical objects or planetary atmospheres to biomedical imaging [3–5]. One of the key components of any application is the source. Until now THz gas lasers have been used in many applications [3, 4]. However, they are not tunable in frequency and can be quite bulky. Due to the prime importance there are many approaches to the development of alternative THz sources. They can be roughly divided into four groups. One approach is based on the extension of microwave technology, i.e. some kind of microwave oscillator (e.g., backward wave oscillator, Gunn diode or YIG oscillator), which is multiplied to the required frequency. The highest frequency generated with these sources is 1.9 THz with an output power of 20 μ W [6]. By downconversion of the radiation from two infrared lasers it is possible to generate about 1 μ W up to 1 THz; above this frequency the emitted power drops down rapidly [7]. Recently a new type of THz laser, the THz quantum cascade

laser (QCL), has been developed [8]. The lasing mechanism is based on interminiband transitions in the conduction band of GaAs/AlGaAs quantum-well heterostructures. Laser operation in the frequency range 1.9–4.8 THz at temperatures of up to \sim 140 K, and high output power of up to 90 mW have been achieved. The fourth approach is based on single crystalline material. Lasing has been demonstrated in p-type germanium in crossed electric and magnetic fields and in uniaxially stressed germanium [9]. More recently, population inversion and lasing have been achieved on intracentre impurity transitions in silicon doped by group-V donors [10].

This paper deals with bulk germanium and silicon THz lasers. The properties of such lasers depend upon the characteristics of the impurities and the properties of the host material into which they are introduced. These characteristics are discussed in terms of their basic physics and the laser performance. The paper is organized as follows. In the first part, three different types of germanium lasers are discussed: the intervalence band (IVB) laser, the cyclotron resonance (CR) laser, and the shallow acceptor laser based on stressed p-germanium. The second part describes recently developed silicon lasers. A number of reviews have been published on germanium lasers [9, 11, 12]. In order to avoid undue repetition the major emphasis in this paper is given on silicon lasers.

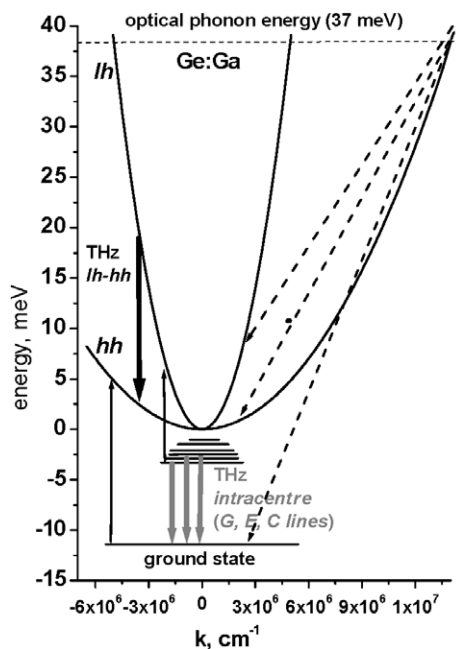


Figure 1. Scheme of optical transitions in Ge:Ga lasers: dashed arrows—relaxation of holes due to interaction with optical phonons; bold black downward arrow—stimulated emission from light- to heavy-hole subband; bold grey downward arrow—stimulated emission on intracentre transition; straight upward arrow—photoionization of Ga states.

2. Germanium lasers

2.1. Intervalence band laser

When hot holes in germanium are subjected to an electric field, E , which is perpendicular to a magnetic induction, B , population inversion and amplification on direct optical transitions between light-hole and heavy-hole subbands of the germanium valence band can occur at cryogenic (up to 80 K) temperatures (figure 1). Often this is referred to as crossed electric and magnetic fields. A strong interaction of the holes with optical phonons is important for this type of laser. At low lattice temperatures (<20 K) the scattering rate of holes having a kinetic energy below the optical phonon energy ($E_{op} = 37$ meV) is relatively low (10^{10} – 10^{11} s $^{-1}$) and controlled by the interaction with acoustic phonons. On the other hand, above the optical phonon energy holes emit optical phonons very rapidly with a rate of 10^{12} s $^{-1}$. As a result a highly anisotropic distribution of hot carriers in momentum space exists when a strong electric field accelerates holes up to the optical phonon energy. Above the optical phonon energy carriers lose their energy and accelerate again. This is called streaming motion. The existence of light-hole and heavy-hole subbands and the presence of a magnetic field, B , in addition to the electric field, E , is essential for p-germanium laser action. In velocity space, the trajectory of holes in crossed electric and magnetic fields is represented by a cyclotron path centred at E/B . When the holes have a small drift velocity $E/B < v_{ol,oh}$, where $v_{ol,oh}$ are the velocities of light and heavy holes with energy E_{op} , their kinetic energy is below the optical phonon energy and they do not emit optical phonons. On the other hand, in fields for which $E/B > v_{ol,oh}$ both

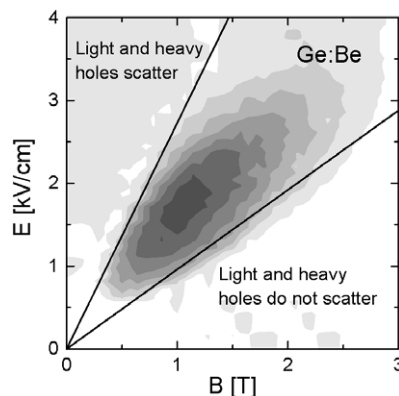


Figure 2. Lasing zone of a Ge:Be laser in E – B space. The grey scale corresponds to the emitted power (darkest grey: highest power).

light and heavy holes reach the energy of the optical phonon and scatter. Note that the probability of scattering any hole into the light-hole or heavy-hole subband by emission of an optical phonon depends only on the density of final states. The effective mass ratio of heavy and light holes is approximately 8, resulting in a higher kinetic energy for heavy holes than for light holes for the same E and B fields. For an appropriate E/B ratio ($v_{ol} > E/B > v_{oh}$) only heavy holes have sufficient kinetic energy and can emit optical phonons. In this situation, optical phonon scattering leads to population inversion and amplification on optical transitions between the light-hole and heavy-hole subbands.

The first observation of stimulated emission from an IVB transition was reported 20 years ago in 1984 [13]. Subsequently, other groups confirmed this observation [14–16]. In order to obtain laser action an electric field of ~ 1 – 2 kV cm $^{-1}$ and a crossed magnetic field of ~ 1 – 2 T have to be applied (figure 2). The most widely used laser design is a rectangular parallelepiped with Ohmic electrical contacts on two of the longest opposite sample facets. The most common field geometry is the Faraday configuration, i.e., the magnetic field is applied along the optical axis of the laser. In this case a superconducting solenoid is usually used for generating it. In the Voigt configuration the magnetic field is transverse to the optical axis. In this case permanent magnets as well as conventional electromagnets can be used. The Voigt set-up with permanent magnets allows a very compact design of the laser in combination with a mechanical cryo-cooler [17]. Several authors indicate a better laser performance and higher gain in the Voigt configuration [18, 19].

IVB lasers have relatively low gain: 0.01 – 0.03 cm $^{-1}$. The main reasons are a low pumping rate (only 4% of scattered heavy holes populate the light-hole subband), short life time (3×10^{-11} s) of the carriers in the upper laser level determined by acoustic-phonon-assisted scattering [20], absorption by free carriers and impurity-to-continuum transitions [21, 22], and multiphonon lattice absorption. Additionally, electron–electron and impurity scattering limit the doping level to 10^{15} cm $^{-3}$ [20]. As a consequence the gain is ~ 0.015 cm $^{-1}$ for Ge:Ga and ~ 0.025 cm $^{-1}$ for Ge:Be with an amplification cross section of $(2$ – $4) \times 10^{-16}$ cm 2 [22, 23]. The optimal doping concentration is 10^{14} – 10^{15} cm $^{-3}$ [24, 25]. The laser performance depends strongly on the homogeneity of the

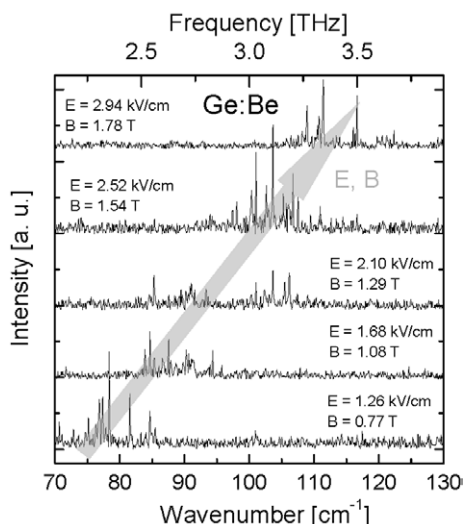


Figure 3. Emission band and tunability of a Ge:Be laser as a function of electric and magnetic fields.

electric field in the laser crystal, which is determined by the Hall effect [26], local doping imperfections and crystal anisotropy [26, 27]. The strong electric fields lead to high current densities in the active part of the laser sample and subsequent heating, which limits both the gain and the duration of lasing. The crystallographic orientation with respect to the electric and magnetic fields also influences the laser operation [27]. From a more practical point of view the $\langle 110 \rangle$ orientation with the magnetic field parallel to the $\langle 110 \rangle$ direction is favourable allowing operation both on IVB and cyclotron resonance transitions [28]. Despite the low gain the IVB germanium laser can reach quite high output power. Depending on the crystal volume, the resonator design and the applied fields output powers between a few tens of a mW up to 10 W have been reported (see [11] and references therein). This corresponds to a conversion efficiency of 10^{-6} – 10^{-4} .

Without any cavity selection the IVB germanium laser has a broadband (10 – 30 cm^{-1}) multi-mode emission, which is tunable in the range of 1 – 4 THz (30 – 140 cm^{-1}) by the applied fields (figure 3). The actual emission spectrum depends on the dopant. IVB lasing has been successfully demonstrated from p-germanium with different group-III acceptors. Originally it was gallium (Ga). Other acceptors are Tl [29], Al [24] and In [30]. These shallow acceptors absorb on impurity-to-continuum transitions in the 11 – 13 meV emission band of the IVB laser, which decreases the gain and causes a gap in the laser spectrum. In order to eliminate this effect, germanium was doped with double acceptors (Be, Zn) instead [25]. Contrary to shallow acceptors the ionization energies of Be and Zn are larger (25 meV and 33 meV, respectively) and well above the energy of the IVB laser emission. In this context THz laser emission from crystals with copper doping (Ge:Cu) was investigated. This kind of laser requires larger doping levels ($1.5 \times 10^{15} \text{ cm}^{-3}$) because only a small fraction of the copper acceptors is ionized by the applied electric field needed for laser operation [31]. Thus the efficiency of acceptor ionization limits the usage of deeper impurities. The optimal balance between the reduction of the absorption related to the impurity centre and sufficient free hole

concentration is found for Ge:Be with a doping concentration $\sim 10^{14}$ – 10^{15} cm^{-3} [22, 25].

An interesting feature of p-germanium lasers doped by group-III acceptors to a level of about 10^{14} cm^{-3} is the occurrence of stimulated emission on transitions between excited states and the ground state of the acceptor (figure 1) [32, 33]. Spectral measurements revealed a characteristic discrete structure which was attributed to impurity transitions related to the G (1.6 THz), E (1.9 THz) and C (2.2 THz) lines of Ga [32, 33]. It was supposed that stimulated IVB emission leads to the depletion of the ground state resulting in population inversion and amplification on transitions from the excited states to the ground state [27, 32, 33].

The axial mode separation depends on the active crystal length and is typically of a few GHz. The width of the order of 1 MHz of a single mode is defined by the duration of the emission pulse (1 – 4 μs) and has been measured by heterodyne spectroscopy [34]. Different schemes for intracavity mode selection and frequency tunability have been employed. By incorporating a mechanically variable lamellar grating or Fabry–Perot resonator into the laser cavity continuous tuning over the emission band and a significant increase in the spectral density have been achieved [35, 36]. Single mode laser operation has been demonstrated using a Fabry–Perot selector [37]. Intracavity wavelength selection has also been achieved by applying a silicon etalon and a dielectric SrTiO₃ selective mirror [38].

Recent work on the IVB germanium laser focuses on two goals: to achieve continuous wave (cw) operation and to generate ultra-short emission pulses. The main limitation to achieving cw operation is the energy dissipated in the crystal. In the early Ga doped lasers overheating occurred after a few microseconds limiting pulse length as well as the repetition rate. Boron-implanted Pd/Au contacts with less contact resistance and an improved contact geometry, which yields better field distribution, enabled longer pulses of stimulated emission [39]. Finally, Ge:Be laser crystals with a volume as small as 0.5 mm^3 and an optimized heat sinking allow higher repetition rates [24, 40]. These improvements have led to a laser duty cycle of 5% and THz emission under continuous electrical excitation which indicates cw optical gain [40].

Since the IVB p-germanium laser emission covers a broad spectral band it is possible to achieve short pulse generation using mode-locking techniques. In particular, one can use active mode-locking and modulate the gain of the IVB germanium laser by means of an additional electric field applied parallel to the magnetic field. This decreases the lifetime as well as the population of the light-hole subband. As a result population inversion is destroyed. If the parallel electric field is modulated at a radio frequency (rf) corresponding to twice the round-trip time of the laser radiation, the gain is at its maximum each time the rf field passes through zero, and it is at its minimum each time the rf field passes through its extremes. Since the gain is modulated mode-locking is induced [41, 42]. Gain modulation is possible in Voigt [41, 42] as well as in Faraday configurations [43] and active mode-locking has been demonstrated with Ga doped as well as Cu doped laser crystals. Pulses as short as 60 ps were generated. The pulse length was limited by the number of equidistant laser modes. In addition, pulse separation from a

mode-locked laser [45] and evidence for passive mode-locking have been obtained [46].

2.2. Cyclotron resonance laser

Under the conditions which provide IVB lasing but in stronger magnetic fields, population inversion can be achieved between certain Landau levels of the light holes. Since the drift energy of the light holes is about equal to their cyclotron energy, Landau quantization and scattering related to light-hole Landau levels with low quantum numbers, n , affect the emission spectra. Population inversion on light-hole to light-hole Landau level transitions can appear due to strong mixing of the light- and heavy-hole states. Strong hybridization of lower lying light-hole Landau states with heavy-hole states at particular fields leads to selective tunnelling of light holes into the heavy-hole subband. This tunnelling is more pronounced for light-hole Landau levels with low quantum numbers than for light-hole Landau levels with large quantum numbers, resulting in population inversion between higher and lower light-hole Landau levels. Landau amplification/absorption for $n \geq 3$ transitions coexists with the broadband light-hole to heavy-hole IVB spectra, while the lines with $n = 1, 2$ appear at higher ($B > 2$ T) magnetic fields. When operated in this mode the laser is called a cyclotron resonance (CR) laser. The first CR laser effect was observed in 1983 [47]. The frequency band of stimulated CR emission is narrow (< 0.2 cm⁻¹) and can be tuned by the magnetic field from 28 cm⁻¹ to 90 cm⁻¹ (0.84–2.7 THz) for the Ge:Ga laser [48, 49] and from 60 cm⁻¹ to 95 cm⁻¹ (1.8–2.85 THz) for the Ge:Zn laser [50]. In general, a couple of CR transitions can act simultaneously and transitions between different light-hole Landau levels with the same quantum number m_j (e.g., $2 \rightarrow 1$ and $1 \rightarrow 0$ [49]) or between levels from different m_j sets are possible [50]. CR lasers require relatively high fields ($B > 2$ T), low doping levels ($< 10^{14}$ cm⁻³) and are strongly dependent on the orientation of the crystallographic axes (the favourable optical axis is $\langle 110 \rangle$) [28]. An output power of ~ 500 mW has been measured [48].

2.3. Stressed germanium laser

Another way to achieve population inversion in p-germanium is to lift the degeneracy in the valence band by applying a compressive force to the germanium crystal. Pulsed stimulated emission has been obtained from stressed (> 4 kbar along $\langle 111 \rangle$ or $\langle 100 \rangle$) Ge:Ga samples (doping concentration $\sim 10^{14}$ cm⁻³) at liquid helium temperatures with an electric field > 2 kV cm⁻¹ [51]. The emission consists of a set of discrete lines with the actual frequency depending on the amount of stress (from 5 THz at 7 kbar to 10 THz at 12 kbar) [52, 53]. The experiments indicate that impurity-related transitions are responsible for the laser effect. Transitions between a so-called ‘resonant impurity state’ of Ga, i.e., a state bound to the split-off heavy-hole subband, and an excited Ga state localized below the valence band [54] are involved. It is supposed that ballistically accelerated light holes are efficiently captured by the resonant states which are inversely populated with respect to the localized Ga states [55]. Recently, it has been reported that this mechanism leads to cw operation at 2.5 THz [54]. However, a detailed

theoretical model and more thorough experiments are needed for a complete understanding of the mechanism.

3. Silicon lasers

3.1. Group-V donors in silicon

Group-V donors are substitutionally incorporated into the silicon host lattice. The energy spectrum of localized impurity states originates from the six equivalent valleys along the $\langle 100 \rangle$ orientations in the energy structure $E_v(\mathbf{k})$ of the conduction band (for a review see [56]). On the basis of the single valley effective mass theory (EMT) with a spherically symmetric Coulomb potential an energy spectrum similar to that of atomic hydrogen but with frequencies falling into the THz range is expected. In the single valley EMT the eigenstates are at least sixfold degenerate due to the six conduction band minima. The deviation from the spherically symmetric potential in the immediate vicinity of the donor site due to the chemical nature of the donor lifts the degeneracy of the $1s(A_1+E+T_2)$ state and resolves it into $1s(A_1)$, $1s(E)$, and $1s(T_2)$ states. This decomposition is called valley-orbit or chemical splitting. The $1s(A_1)$ state with the largest amplitude at the donor site is strongest affected by chemical shift and splitting. For the p-like states the wavefunction yields a small probability near the donor site and consequently the splittings are too small to be experimentally observable.

For low lattice temperatures the lifetime of an electron in a particular donor state is determined by the interaction with phonons. The characteristics of the impurity states and phonon spectra determine the laser emission. Principally, two mechanisms for population inversion in silicon doped by group-V impurities can be distinguished. One mechanism is based on the accumulation of charge carriers in long-lived bound excited states of neutral donors while the other is based on a resonant electron-phonon interaction.

3.2. Lasing based on long-lived impurity states

For all group-V donors in silicon except Bi the $2p_0$ state is long lived. At low lattice temperatures ($T < 30$ K) the interaction with intervalley optical and acoustic and intravalley optical phonons is negligible for these centres. Therefore, the population of the excited states is controlled by long-wavelength acoustic-phonon-assisted relaxation (figure 4). Population of the intracentre states can be achieved by either optical excitation into the conduction band (intraband excitation or photoionization) [57, 58] or by resonant optical excitation into one of the excited states (intracentre excitation) [59]. In the first case, optically excited carriers lose their energy through the interaction with acoustic or optical phonons in the conduction band (figure 4). Which type of relaxation prevails depends on the energy of the pump photons. If their energy is large enough relaxation in the conduction band is mainly achieved by optical phonons, otherwise acoustic phonons dominate. Further on, the excited carriers are captured by ionized impurity centres and relax through the excited impurity states with a characteristic step $\delta E = (8E_i m^* s^2)^{1/2}$ [60], where s is the velocity of sound, m^* is the effective electron mass, and E_i is the ionization energy of the impurity

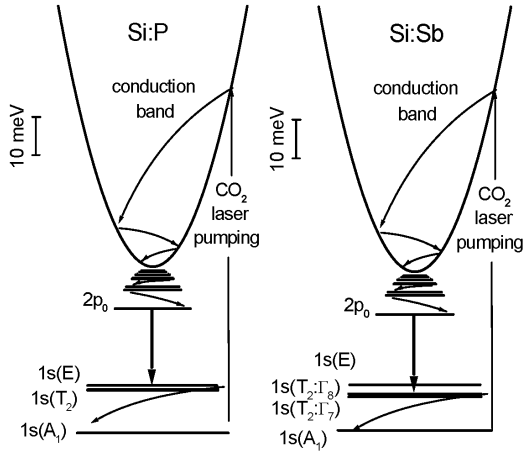


Figure 4. Energy level schemes and lasing principle of Si:P (left) and Si:Sb (right) lasers.

state i . The quasi-classical density of states of Coulomb centres drops with increasing ionization energy as $E_i^{-5/2}$. The lower excited states are separated by energy gaps $\Delta E > \delta E$. The rate of acoustic-phonon-assisted transitions between such states decreases not slower than $(\Delta E/\delta E)^{-5}$ [61]. Except for Bi the $2p_0$ state is long lived, since intravalley phonons cannot contribute to the de-excitation to the $1s(E)$ and $1s(T_2)$ states because of energy and momentum conservation. Calculations that take into account inter- and intervalley acoustic-phonon-assisted relaxation yield values of the order of 10^{-9} s and 10^{-10} – 10^{-11} s for the lifetime of the carriers in the $2p_0$ and $1s(E)$, $1s(T_2)$ states, respectively [62, 63]. This leads to an accumulation of the photoexcited carriers in the $2p_0$ state and the formation of a population inversion between this state and the lower $1s(E)$ and $1s(T_2)$ states [64]. Consequently, a four-level laser scheme is realized and lasing can occur on the $2p_0 \rightarrow 1s(E)$, $1s(T_2)$ transitions. Silicon doped by P and by Sb are two examples of this type of laser. One important difference between them is caused by the higher atomic number of Sb compared to P. This results in a noticeable spin-orbit splitting of the $1s(T_2)$ state into the doublet $1s(T_2:\Gamma_7)$ and quadruplet $1s(T_2:\Gamma_8)$ separated by 0.3 meV (figure 4).

Si:P and Si:Sb crystals as well as Si:Bi and Si:As, which will be discussed below, were float-zone or Czochralski grown and doped in the range $N_P = (0.9\text{--}7) \times 10^{15}$ cm $^{-3}$ (Si:P, Si:Sb, Si:As) or $>10^{16}$ cm $^{-3}$ (Si:Bi). The ingots were cut into parallelepipeds with typical dimensions of $7 \times 7 \times 5$ mm 3 . The end facets were polished with an accuracy of ~ 1 arcmin in order to provide a high- Q resonator on internal reflection modes. The crystals were cooled below 30 K either by immersing them into liquid helium or by means of a mechanical cryo-cooler and optically excited by a TEA CO $_2$ laser. The output emission was spectrally analysed with a Fourier transform spectrometer (FTS).

A Si:P laser has a single emission line at 5.41 THz (180.66 cm $^{-1}$, 22.39 meV) (figure 5) [10, 65]. Its frequency is in excellent agreement with the transition from the $2p_0$ state to the $1s(T_2)$ state as measured by Fourier transform spectroscopy [66]. A laser transition to the $1s(E)$ state was not observed. Two competing factors determine the relative gain of the $2p_0 \rightarrow 1s(T_2)$ and $2p_0 \rightarrow 1s(E)$ transitions. On the one hand,

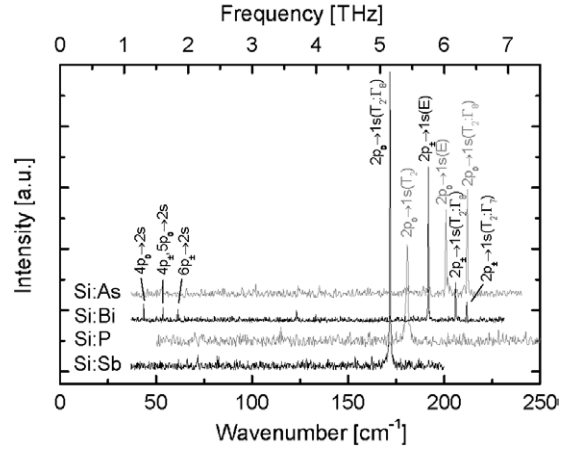


Figure 5. Emission spectra of silicon lasers doped by group-V impurities optically excited by radiation from a CO $_2$ laser. The spectra were measured with an FTS and a resolution of 0.2 cm $^{-1}$.

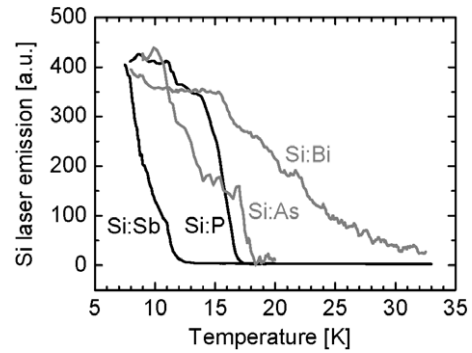


Figure 6. Laser emission as a function of silicon lattice temperature. The lasers are optically excited by radiation from a CO $_2$ laser.

the acoustic-phonon-assisted relaxation of carriers from the $1s(E)$ state is faster than that from the $1s(T_2)$ state because group theory considerations allow only intervalley phonons for the $1s(T_2) \rightarrow 1s(A_1)$ transition, whereas both intravalley and intervalley phonons contribute to relaxation from the $1s(E)$ state [67]. On the other hand, the optical cross section for the transition from the $2p_0$ state to the triplet $1s(T_2)$ state is about 1.5 times larger than that to the doublet $1s(E)$ state [66]. For a Si:P laser the latter factor dominates and determines the laser action [68, 69]. Similarly, the emission from a Si:Sb laser consists of a single line at 5.15 THz (171.8 cm $^{-1}$, 21.31 meV) (figure 5) [70]. This corresponds to the $2p_0 \rightarrow 1s(T_2:\Gamma_8)$ transition and is in very good agreement with Lyman spectra that yield 21.32 meV [66]. The spin-orbit splitting modifies the optical cross sections as compared to Si:P. Therefore the $2p_0 \rightarrow 1s(T_2:\Gamma_8)$ transition dominates. The Si:P laser can operate up to 17 K while in Si:Sb laser action ceases at 12 K (figure 6).

3.3. Lasing based on resonant electron-phonon interaction

This laser mechanism is due to the resonant interaction of certain impurity states with optical phonons. One example is Si:Bi. For this medium the $2s$ and $2p_0$ states are resonantly coupled to the $1s(A_1)$ ground state by optical phonons [71]. At temperatures where the thermal energy is much smaller than

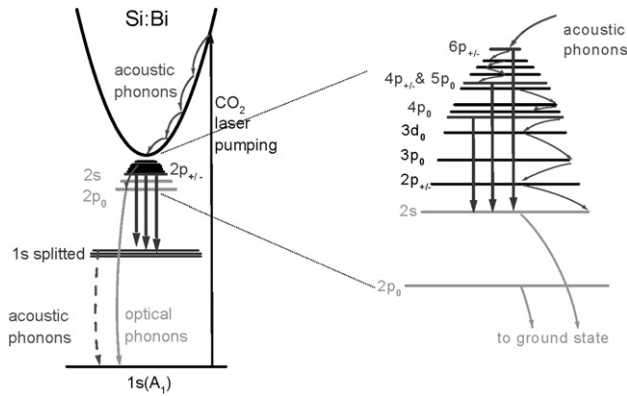


Figure 7. Energy levels and lasing transitions (straight downward arrows) in Si:Bi. On the left-hand side, the short wavelength transitions from $2p_0$ to the split $1s(E,T)$ states are shown. On the right-hand side, laser transitions from higher excited states that end in the $2s$ state are shown.

the energy of the optical phonons spontaneous emission of transverse (TO g-type, 62 meV, TO f-type, 59.1 meV) optical phonons [72] depopulates the $2s$ and $2p_0$ states via a direct transition to the $1s(A_1)$ ground state (figure 7). This results in a lifetime of about 1 ps for these states. In short, the mechanism is as follows. Optically excited free carriers lose their energy through interaction with acoustic and optical phonons in the conduction band until they are captured by ionized impurity centres. This process is followed by an acoustic-phonon-assisted cascade capture essentially in the same way as for Si:P or Si:Sb. Once a free carrier arrives at the $2s$ or $2p_0$ state the situation is different. Due to the resonant interaction the majority of the optically excited electrons relax directly from these states to the $1s(A_1)$ ground state leaving the $1s(E)$ and $1s(T_2)$ states essentially unpopulated. Carriers are trapped in these states only by optical-phonon-assisted recombination from the conduction band or direct acoustic-phonon-assisted transitions from the $3s$ state. The probability of populating the $2p_{\pm}$ state via cascade relaxation is calculated to be about 0.5, while for the $1s(E)$ and $1s(T_2)$ states it is about 100 times less. Although the lifetime of the $2p_{\pm}$ state and the lower $1s(E)$ and $1s(T_2)$ states is almost the same (~ 100 ps), the latter are essentially unpopulated. In principle, population inversion can be achieved between states higher than the $2s$ state and the $2p_0$, $1s(E)$ and $1s(T_2)$ states. For transitions, which end in the $1s(E)$ or $1s(T_2)$ state, an amplification of $0.1\text{--}1\text{ cm}^{-1}$ on $2p_{\pm} \rightarrow \{1s(T_2), 1s(E)\}$ transitions was calculated for a Bi concentration of $2 \times 10^{15}\text{ cm}^{-3}$, a pump photon flux density $> 10^{22}\text{ cm}^{-2}\text{ s}^{-1}$ and a temperature of 4 K. For transitions ending in the $2s$ or $2p_0$ states, an amplification of the order of $0.01\text{--}0.1\text{ cm}^{-1}$ was calculated for Si:Bi with a Bi concentration of 10^{16} cm^{-3} , a pump photon flux density $> 10^{22}\text{ cm}^{-2}\text{ s}^{-1}$ and temperatures below 80 K [58, 69].

Due to the high atomic number of Bi the spin-orbit splitting of the $1s(T_2)$ state into the doublet $1s(T_2:\Gamma_7)$ and quadruplet $1s(T_2:\Gamma_8)$ states is about 1 meV, much larger than for other group-V donors [66]. This modifies the optical cross sections making the $2p_{\pm} \rightarrow 1s(T_2:E)$ the dominant emission line. Thus, there are three emission lines with the $2p_{\pm}$ state as the upper level and the $1s(E, T)$ states as the lower level (figure 5) [69, 73]. In addition three long-wavelength laser

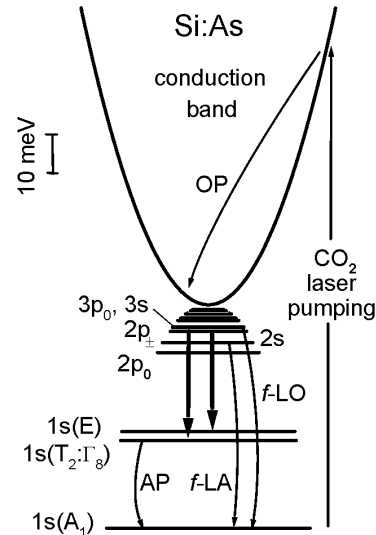


Figure 8. Schematic of the Si:As four-level laser scheme when optically excited by radiation from a CO_2 laser: AP and OP are acoustic and optical phonon-assisted relaxation processes. Lasing transitions are $2p_{\pm} \rightarrow \{1s(E), 1s(T_2)\}$. Other symbols are the notation of the excited As donor states.

lines have been observed and identified to be from transitions between higher excited states and the $2s$ state [69]. All emission frequencies are in excellent agreement with the data obtained from Lyman spectra. The 30 K operation temperature of the Si:Bi laser is the highest of all silicon lasers.

The other example is silicon doped with arsenic (Si:As). It is of particular interest because on the one hand the $2p_0$ state is long lived, similar to Si:P, and on the other hand the LA f-phonon, which transfers an electron in a $\langle 110 \rangle$ -type direction to one of the four equivalent valleys, has an energy close to the gap between the As impurity ground state and $2s$ and $2p_{\pm}$ states. The latter is similar to the situation in Si:Bi. The population inversion in Si:As is maintained as follows (figure 8). At low lattice temperatures electrons are excited from the $1s(A_1)$ state to the continuum and relax to the bottom of the conduction band by a similar cascade process as for the other dopants. This cascade process ends when the carriers reach the $2s$ state. The arsenic $2s$ state is split into three levels: Γ_1 , Γ_5 and Γ_3 . The $2s(E:\Gamma_3)$ state is coupled to the $1s(A_1)$ ground state by intervalley LA f-phonons with an energy of 46.3 meV. This is one of the strongest electron-phonon interactions in silicon since it is allowed by group-theoretical analysis [72]. The characteristic rate of such a process is $10^{11}\text{--}10^{12}\text{ s}^{-1}$ and carriers captured in the $2s$ state do not reach the $2p_0$ and $1s(E)$, $1s(T_2)$ states. The lifetime of the latter states is estimated to be $\sim 10^{-10}\text{--}10^{-11}\text{ s}$ [62]. Coupling of the $3s$ and $3p_0$ states to the As ground state via the f-LO phonon (48.8 meV) is a much weaker process [72] and does not completely interrupt the cascade-type population of the $2p_{\pm}$ state. However, this shortcut lowers the gain of the laser. As a result, population of the $2p_{\pm}$ state is highest and lasing arises on the $2p_{\pm} \rightarrow 1s(E), 1s(T_2)$ transitions at 5.87 THz ($24.94 \pm 0.02\text{ meV}$) and 6.64 THz ($26.33 \pm 0.02\text{ meV}$), respectively [74]. These values differ slightly from those deduced from absorption measurements for Si:As at $\sim 60\text{ K}$ ($24.86 \pm 0.01\text{ meV}$ and $26.29 \pm 0.01\text{ meV}$) [66]. The difference of

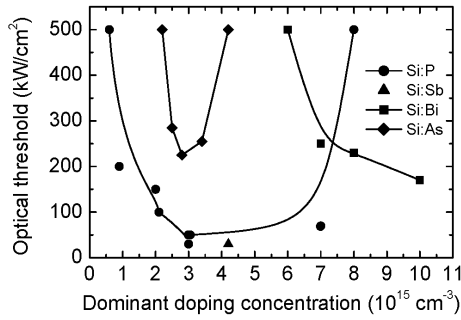


Figure 9. Laser threshold as a function of doping concentration for intraband excitation with a CO₂ laser. The values at 500 kW cm⁻² are lower limits. For these samples only spontaneous emission was observed.

0.04–0.08 meV is very likely caused by thermal broadening of the impurity states in the absorption measurements. In contrast to Si:Bi no emission has been observed on the long wavelength $\{np_0, np_{\pm}\} \rightarrow 2s, n = 3, 4, \dots$ transitions, because the resonant phonon interaction in Si:As is less efficient. The maximum operation temperature is 20 K (figure 6).

3.4. Laser threshold and D⁻ centres

The lowest laser threshold for Si:P and Si:Sb lasers is about 40 kW cm⁻² ($\sim 2 \times 10^{24}$ photons cm⁻² s⁻¹) and the output power reaches several mW. With 100 kW cm⁻² ($\sim 5 \times 10^{24}$ photons cm⁻² s⁻¹) the threshold of Si:Bi lasers is significantly higher. This reflects the less efficient population inversion mechanism. The output power of these lasers is less than 1 mW. Achieving cw operation does not appear very promising. The limiting factors are the short lifetimes of the involved states, efficiency of the cascade capture, and heating of the crystal by the pump radiation. The optimum net doping concentration is about 5×10^{15} cm⁻³ for lasers based on the long-lived 2p₀ state (figure 9). Below this concentration the gain decreases due to the decreasing number of donors, while above it impurity broadening of the energy levels starts to become important; this lowers the peak value of cross section for the particular intracentre transition and results in lower gain and a higher laser threshold. Compensation of the dominant dopant by acceptor centres has a positive effect on the laser threshold, i.e., the laser threshold for intraband excitation is about a factor of 2 lower for lasers compensated by $\sim 30\%$ than for uncompensated ones (figure 10) [75]. The compensation closes one channel of losses that arise from the absorption of THz radiation by D⁻ centres. In an uncompensated n-silicon crystal photoexcited electrons can be captured by neutral donors and form negatively charged D⁻ centres [77]. These centres have a large absorption at THz frequencies. If the compensation is chosen properly the free electrons are captured predominantly by the positively charged donors and the formation of D⁻ centres is negligible. Si:As is somewhat peculiar. The laser threshold is the highest of all lasers (200–250 kW cm⁻², $\sim 10^{25}$ photons cm⁻² s⁻¹). The optimum doping concentration of As donors is $(2.5\text{--}3.5) \times 10^{15}$ cm⁻³, close to the value for Si:P and Si:Sb lasers. Lower and higher doped samples exhibit merely spontaneous emission. The optimum doping concentration differs by about one order of magnitude from the optimum doping for Si:Bi

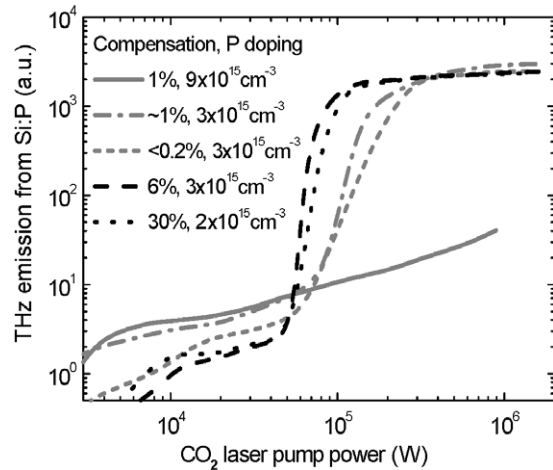


Figure 10. Laser threshold of Si:P lasers with different degrees of boron compensation when optically excited by radiation from a CO₂ laser. The samples with a compensation of 6% and 30% have about 30% lower threshold than the uncompensated samples. This can be attributed to the suppression of absorption by D⁻ centre.

($\geq 1 \times 10^{16}$ cm⁻³) [77]. These peculiarities are due to the resonant phonon interaction which is weaker than for Si:Bi but sufficiently strong to inhibit a Si:P or Si:Sb-like laser process with 2p₀ as the upper laser state.

3.5. Frequency tunability

The frequency can be tuned by applying either a magnetic field or external stress. The degeneracy of certain shallow donor states is lifted when a magnetic field is applied [78]. This results in a splitting and a shift of the states (Zeeman effect). At low magnetic fields (typically below 3–4 T) shift and splitting grow linearly with the magnetic field. For Si:P no change of the emission frequency or power up to 2 T has been observed. For Si:Bi both laser transitions split symmetrically around the zero field frequency (for $B \parallel \langle 112 \rangle$). The splitting is 0.08 meV T⁻¹ (20 GHz T⁻¹ = 0.3% T⁻¹). The laser emission disappears at a field between 0.5 T and 1.0 T, where the overlap of the gain profiles of both transitions is not sufficient to maintain laser action. From this the width of the gain profile can be estimated to be about 1.5 cm⁻¹.

When external stress is applied to a crystal the energy band extrema shift. In general, the symmetry of a crystal is lowered. This results in the lifting of degeneracies associated with the band extremes and the energy levels of an impurity [79]. The dependence of donor levels on external stress can be calculated using perturbation theory. For a compressive force parallel to $\langle 100 \rangle$ the 1s(E) $\rightarrow np$ transitions split into three components: one shifts to lower frequency, one to higher frequency, and one stays constant. The 1s(T₂) $\rightarrow np$ transitions do not split because the lower and the upper state change their position with the same rate. For other directions of stress the splitting of the levels is qualitatively the same. No frequency shift exists for the 2p₀ \rightarrow 1s(T₂) laser transition of Si:P for a compressive force applied along $\langle 100 \rangle$. In contrast, the 2p_± \rightarrow 1s(T₂;Γ₈) transition of the Si:Bi laser shifts by 6 cm⁻¹/kbar (180 GHz kbar⁻¹ = 3% kbar⁻¹) towards higher frequencies for stress applied along $\langle 112 \rangle$ or $\langle 110 \rangle$.

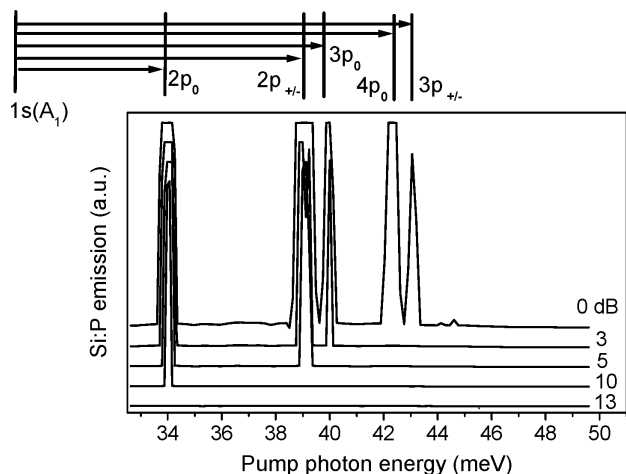


Figure 11. Emission of the Si:P laser as a function of pump photon energy and pump power from the free electron laser. The attenuation of pump radiation is given in dB relative to maximum power. Laser emission appears when the pump photon energy coincides with the photoexcitation of the impurity centre.

3.6. Intracentre excitation

An alternative means of optical excitation is intracentre pumping. In this case, the electrons are pumped directly into one of the bound excited impurity states. Intracentre excitation differs from intraband excitation in several aspects. First of all, the optical absorption cross sections of intracentre transitions are about two orders of magnitude larger than those of impurity-to-band transitions far in the conduction band ($\sim 10^{-14}$ cm² instead of $\sim 10^{-16}$ cm²) [66]. Secondly, the de-excitation of electrons from the band leads to heating of the silicon lattice which in turn changes the spectral density of acoustic phonons and affects the population inversion as well as the absorption of THz radiation. Last but not least, the gradual relaxation of the electrons in the band and the higher excited impurity states leads to the creation of shallow D⁻ centres as discussed above. Thus, intracentre excitation of group-V donors in silicon is the more efficient optical pumping scheme. Stimulated emission by intracentre excitation has been observed from all silicon lasers described above. As an example we will discuss Si:P and Si:Bi lasers under intracentre optical excitation [59, 80].

The measurements were made using the frequency tunable (15–40 μ m) free electron laser for infrared experiments (FELIX) at the FOM Institute in Rijnhuizen, the Netherlands. The pump radiation consisted of 6–8 μ s long trains of micropulses (6–8 ps FWHM, 1 ns separation, peak power ~ 0.5 MW) at a repetition rate of 5 Hz. The average power of this macropulse was ~ 2.5 kW. The scans were performed with a discrete wavelength step of 0.02 μ m. The bandwidth of the FEL laser pulse was ~ 0.5 –1% of the central wavelength.

Laser emission from Si:P was obtained when the pump energy corresponded to intracentre transitions between the 1s(A₁) ground state and any of the excited states. An example of excitation into odd-parity states is shown in figure 11. Excitation into states higher than 2p₀ results in emission on the 2p₀ \rightarrow 1s(T₂) transition similar to intraband excitation with a CO₂ laser. For direct excitation into the 2p₀ state stimulated

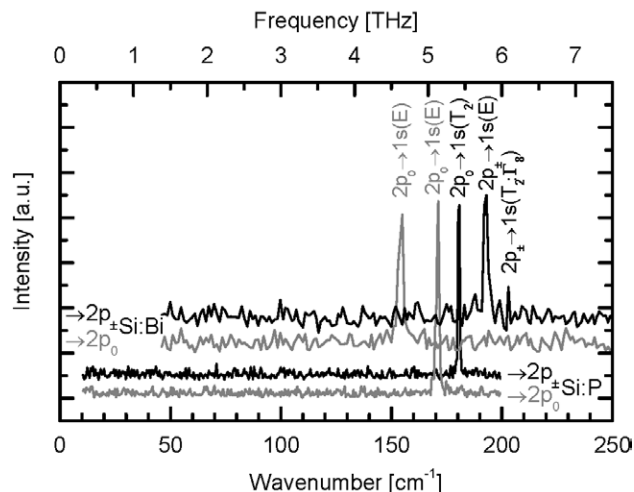


Figure 12. Emission spectra of Si:P and Si:Bi lasers when optically excited with a free electron laser. The spectra were measured with an FTS and a resolution of 0.2 cm⁻¹. Note the change of the emission frequency when the pump state changes from 2p₀ to 2p_±.

emission occurs on the 2p₀ \rightarrow 1s(E) transition at 171 cm⁻¹ (figure 12). Apparently, the lower population of the 1s(E) state resulting from its shorter lifetime determines the laser transition. This compensates for the larger cross section of the 2p₀ \rightarrow 1s(T₂) transition. In the case of Si:Bi stimulated emission has been observed from the same transitions as for intraband excitation, namely the 2p_± \rightarrow 1s(E), 1s(T₂: Γ_8) transitions for all except one pump frequency (figure 12). Compared to intraband excitation another emission line appeared for direct pumping into the 2p₀ state (figure 12). The emission frequency corresponds to the transition from the 2p₀ to the 1s(E) state. Lasing occurs despite the strong resonant-type interaction of the ground state that leads to the fast de-excitation of the 2p₀ state [57]. The very high micropulse peak power available from FELIX leads to an extremely fast pumping rate up to $\sim 10^{13}$ s⁻¹. Even considering the very short pumping time, equal to a single micropulse duration of 6–10 ps FWHM, this is sufficient to achieve population inversion and laser gain.

For intracentre excitation of Si:P the lowest threshold pump power density averaged over the macropulse was ~ 50 W cm⁻² ($\sim 9 \times 10^{21}$ photons cm⁻² s⁻¹). This was achieved for direct excitation into the upper laser level. The Si:Bi laser has the lowest threshold when pumped into the 2p_± state (170 W cm⁻², $\sim 1.6 \times 10^{22}$ photons cm⁻² s⁻¹). Direct excitation into the 2p₀ state has a pump threshold of 1.7 kW cm⁻² ($\sim 2 \times 10^{23}$ photons cm⁻² s⁻¹), which is about one order of magnitude higher than for pumping into the 2p_± state due to the resonant phonon interaction. In general, intracentre excitation is more efficient than intraband excitation.

It is worth noting that in total 17 emission lines have been obtained from intracentre excitation of Si:P (2 lines), Si:Sb (5), Si:Bi (3) and Si:As (7). The appearance of a particular laser transition depends on the state which is pumped and on the pump power. This indicates that the electron–phonon interaction and the spectral density of the phonons in silicon are crucial for the laser process.

3.7. Electrical excitation

It has been suggested that the same principles as for the IVB p-germanium laser can be applied to p-doped silicon in crossed magnetic and electric fields at low lattice temperatures [81]. A hot-hole population inversion in the valence band between light- and heavy-hole Landau levels or within the light-hole Landau levels might be obtainable. The first calculations [82, 83] predicted an emission frequency up to 10 THz and gain at temperatures as high as 77 K. Monte Carlo simulations of hot holes in silicon which take into account the warped valence bands [84] indicate that laser emission is achievable over a wide frequency range from 0.5 to 5 THz and gain with an optimum at $E/B \sim 0.4\text{--}0.8 \text{ kV cm}^{-1} \text{ T}^{-1}$ for $B \sim 3 \text{ T}$. Spontaneous emission in the terahertz range has been observed from a $30 \times 5 \times 4.1 \text{ mm}^3$ silicon crystal doped with a boron concentration of $1.5 \times 10^{15} \text{ cm}^{-3}$. The maximum output was achieved for $B \sim 3 \text{ T}$ at $E/B \sim 0.65 \text{ kV cm}^{-1} \text{ T}^{-1}$ and pulsed electric field [85]. The authors suggest that the observed emission is caused by population inversion between hot holes. However, no laser emission has been observed to date.

Recently, electroluminescence at THz frequencies has been observed from electrically pumped boron doped p-type silicon [86] and phosphor doped n-type silicon [87]. The samples were fabricated from $380 \mu\text{m}$ thick silicon wafers doped to a level of $\sim 10^{15} \text{ cm}^{-3}$. Schottky contacts were used for effective injection of carriers. Electrical pulses with a duration of 250 ns and with a repetition rate of 413 Hz were used for excitation, and the collected power was calculated to be $\sim 20 \mu\text{W}/\text{facet}$ for a $190 \times 120 \mu\text{m}^2$ device with a peak current of 400 mA at 12 K. The emission was observed at electric fields above 1.8 kV cm^{-1} , which is a factor 2.5 larger than the observed current conduction threshold. The intensity of the THz emission increases linearly with current and quenched when the temperature of the sample was above 30 K for Si:P and above 20 K for Si:B. Some radiation was still detectable at temperatures as high as 150 K. The emission spectra show that the observed radiation corresponds to intracentre transitions of impurities in silicon, similar to that for optical excitation [10, 65]. The generation of the electroluminescence is attributed to impact ionization of the neutral impurities in the bulk silicon by the injected electrons.

Whether electrical excitation can eventually result in laser emission is not yet clear. For p-germanium, it has been shown theoretically [33] that impact ionization is not sufficient for this laser mechanism. The depletion of impurity levels in an electric field above the impurity ionization threshold affects mostly excited states with small binding energies. Population of excited states, which are supposed to serve as the upper laser level, might be possible for particular dopants via a fast direct capture of free carriers into the excited states due to scattering on optical phonons of the host lattice. However, this may not overcome the depletion by impact ionization. Thus, electrical excitation of bulk silicon does not seem to be a straightforward approach to realizing a THz intracentre laser. This disadvantage might be overcome in silicon-based heterostructures, where the electron transport and the relaxation via impurity levels can be spatially separated.

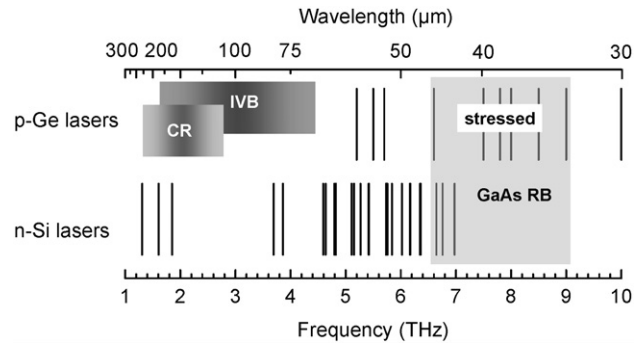


Figure 13. Frequency coverage of silicon and germanium lasers (IVB: light- to heavy-hole intervalence band laser, CR: cyclotron resonance laser). Note that some of the emission lines of the silicon laser fall into the Reststrahlenband (RB) of GaAs.

4. Outlook

Lasers based on bulk germanium and silicon cover a wide range of the THz portion of the electromagnetic spectrum (figure 13). For more than 20 years extensive research has been carried out on p-germanium lasers, which has resulted in a very thorough understanding of the underlying physical mechanisms. However, owing to their complexity, applications of p-germanium lasers are mainly restricted to research laboratories. With the latest technological improvements, a more convenient operation in a closed cycle cooler with permanent magnets is possible and may open the door for more applications. The n-type silicon laser was invented only a few years ago. Within a very short time lasers with different donors and different excitation schemes have been developed. While the principle lasing mechanisms and the involved states have been worked out, a detailed understanding of the electron–phonon interaction that governs the laser mechanism is still missing. It is worth noting that this is the first laser ever realized with silicon. An interesting feature of the silicon laser is that it operates right in the Reststrahlenband of GaAs (figure 13). In this region GaAs/AlGaAs QCLs might not work at all. Therefore it is well worth pursuing the development of this type of laser. In order to extend the frequency coverage of QCLs different research groups work with various designs of SiGe structures, mainly employing intersubband transitions in the quantum-well valence band (see, e.g., [88, 89]). Electroluminescence from the SiGe/Si structures has been obtained at far- and mid-infrared wavelengths. Difficulties encountered are the natural internal lattice mismatch induced strain of the SiGe/Si layers and the short lifetimes of carriers in the upper laser level [90]. One approach might be to incorporate impurities into a SiGe superlattice. Intracentre boron-related electroluminescence has been observed from vertically excited cascade-type p-SiGe:B/Si heterostructures [91]. Another group reported stimulated THz emission from impurity-related transitions from in-plane electrically pumped p-SiGe:B/Si heterostructures [92], but this needs further verification. In summary, germanium and silicon THz lasers remain an exciting field of research mostly from the viewpoint of fundamental physics but also for dedicated applications.

Acknowledgments

This work was supported by the Deutsche Forschungsgemeinschaft and the Russian Foundation for Basic Research (RFBR) (joint grant 436 RUS 113/206/0-3 and 03-02-04010) and RFBR grant 02-02-16790.

References

- [1] Grüner G (ed) 1998 *Millimeter and Submillimeter Wave Spectroscopy of Solids* (Berlin: Springer)
- [2] De Lucia F C 2003 *Sensing with Terahertz Radiation* ed D Mittleman (Berlin: Springer) p 39
- [3] Hübers H-W, Schwaab G W and Röser H P 1996 *ESA SP-388* p 159
- [4] Titz R U, Birk M, Hausamann D, Nitsche R, Schreier F, Urban J, Küllman H and Röser H P 1995 *Infrared Phys. Technol.* **36** 883
- [5] Koch M 2003 *Sensing with Terahertz Radiation* ed D Mittleman (Berlin: Springer) p 295
- [6] Mehdi I 2004 *Proc. SPIE* **5498** 103
- [7] Duffy S M, Verghese S and McIntosh K A 2003 *Sensing with Terahertz Radiation* ed D Mittleman (Berlin: Springer) p 193
- [8] Köhler R, Tredicucci A, Beltram F, Beere H E, Linfield E H, Davies A G, Ritchie D A, Iotti R C and Rossi F 2002 *Nature* **417** 156
- [9] Gornik E and Andronov A A (ed) 1991 *Opt. Quantum Electron.* **23** S111
- [10] Pavlov S G, Zhukavin R Kh, Orlova E E, Shastin V N, Kirsanov A V, Hübers H-W, Auen K and Riemann H 2000 *Phys. Rev. Lett.* **84** 5220
- [11] Bründermann E 2004 *Long-Wavelength Infrared Semiconductor Lasers* ed H K Choi (London: Wiley) p 279
- [12] Gornik E, Rosskopf V and Heiss W 1995 *Infrared Phys. Technol.* **36** 113
- [13] Andronov A, Zverev I V, Kozlov V A, Nozdryn Yu N, Pavlov S A and Shastin V N 1984 *Sov. Phys.—JETP Lett.* **25** 804
- [14] Komiyama S, Iizuka N and Akasaka Y 1985 *Appl. Phys. Lett.* **47** 958
- [15] Mityagin Yu, Murav'ev A V, Murzin V N, Nozdryn Yu N, Pavlov S A, Stoklitskii A A, Trofimov I E, Chebotarev A L and Shastin V N 1986 *Sov. Phys. Lebedev Inst. Rep.* **12** 47
- [16] Helm M, Unterrainer K, Gornik E and Haller E E 1988 *Solid-State Electron.* **31** 759
- [17] Bründermann E and Röser H P 1997 *Infrared Phys. Technol.* **38** 201
- [18] Hosako I and Komiyama S 1992 *Semicond. Sci. Technol.* **7** B645
- [19] Vorob'ev L E, Danilov S N, Kochegarov Yu V, Firsov D A and Tulupenko V N 1997 *Semiconductors* **31** 1273
- [20] Shastin V N 1991 *Opt. Quantum Electron.* **23** S111
- [21] Heiss W, Kremser C, Unterrainer K, Strasser G, Gornik E, Meny C and Leotin J 1993 *Phys. Rev. B* **47** 16586
- [22] Auen K, Hübers H-W, Murav'ev A, Orlova E, Pavlov S, Shastin V N and Zhukavin R 2001 *Physica B* **302–303** 334
- [23] Murav'ev A V, Withers S H, Pavlov S G, Shastin V N and Peale R E 1999 *J. Appl. Phys.* **86** 3512
- [24] Bründermann E, Linhart A M, Röser H P, Dubon O D, Hansen W L and Haller E E 1996 *Appl. Phys. Lett.* **68** 135
- [25] Bründermann E, Linhart A M, Reichertz L, Röser H P, Dubon O D, Hansen W L, Sirmain G and Haller E E 1996 *Appl. Phys. Lett.* **68** 3075
- [26] Strijbos R C, Dijkstra J E, Lok J G S, Schets S I and Wenckebach W T 1994 *Semicond. Sci. Technol.* **9** 6489
- [27] Mityagin Yu A, Murzin V N, Stepanov O N and Stoklitsky S A 1992 *Semicond. Sci. Technol.* **7** B641
- [28] Stoklitskiy S A 1992 *Semicond. Sci. Technol.* **7** B610
- [29] Heiss W, Unterrainer K, Gornik E, Hansen W L and Haller E E 1994 *Semicond. Sci. Technol.* **9** 638
- [30] Murav'ev A V, Pavlov S G and Shastin V N unpublished result
- [31] Sirmain G, Reichertz L A, Dubon O D, Haller E E, Hansen W L, Bründermann E, Linhart A M and Röser H P 1997 *Appl. Phys. Lett.* **70** 1659
- [32] Murav'ev A V, Pavlov S G and Shastin V N 1990 *JETP Lett.* **52** 343
- [33] Murav'ev A V, Pavlov S G, Orlova E E and Shastin V N 1994 *JETP Lett.* **59** 89
- [34] Bründermann E, Röser H P, Murav'ev A V, Pavlov S G and Shastin V N 1995 *Infrared Phys. Technol.* **36** 59
- [35] Murav'ev A V, Nefedov I M, Pavlov S G and Shastin V N 1993 *Quantum Electron.* **23** 119
- [36] Komiyama S, Morita H and Hosako I 1993 *Japan. J. Appl. Phys.* **32** 4987
- [37] Murav'ev A V, Withers S H, Weidner H and Strijbos R C 2000 *Appl. Phys. Lett.* **76** 1996
- [38] Du Bosq T W, Peale R E, Nelson E W, Murav'ev A V, Fredricksen C J, Tache N and Tanner D B 2003 *J. Appl. Phys.* **94** 5474
- [39] Bründermann E, Röser H P, Heiss W, Gornik E and Haller E E 1995 *Appl. Phys. Lett.* **67** 3543
- [40] Bründermann E, Chamberlin D R and Haller E E 2000 *Appl. Phys. Lett.* **76** 2991
- [41] Hovenier J N, Murav'ev A V, Pavlov S G, Shastin V N, Strijbos R C and Wenckebach W Th 1997 *Appl. Phys. Lett.* **71** 443
- [42] Hovenier J N, Klaassen T O, Wenckebach W Th, Murav'ev A V, Pavlov S G and Shastin V N 1998 *Appl. Phys. Lett.* **72** 1140
- [43] Murav'ev A V, Withers S H, Strijbos R C, Pavlov S G, Shastin V N and Peale R E 1999 *Appl. Phys. Lett.* **75** 2882
- [44] Hovenier J N, DeKleijn R M, Klaassen T O, Wenckebach W Th, Chamberlin D R, Bründermann E and Haller E E 2000 *Appl. Phys. Lett.* **77** 3155
- [45] Murav'ev A V, Strijbos R C, Fredericksen C J, Withers S H, Trimble W, Pavlov S G, Shastin V N and Peale R E 1999 *Appl. Phys. Lett.* **74** 167
- [46] Murav'ev A V, Strijbos R C, Fredericksen C J, Trimble W, Withers S H, Pavlov S G, Shastin V N and Peale R E 1998 *Appl. Phys. Lett.* **73** 3037
- [47] Ivanov Yu L and Vasil'ev Yu V 1983 *Sov. Tech. Phys. Lett.* **9** 264
- [48] Unterrainer K, Kremser C, Gornik E, Pidgeon C R, Ivanov Yu L and Haller E E 1990 *Phys. Rev. Lett.* **64** 2277
- [49] Unterrainer K, Kremser C, Wurzer C, Gornik E, Pfeffer P, Zawadzki W, Murdin B and Pidgeon C R 1992 *Semicond. Sci. Technol.* **7** B604
- [50] Reichertz L A, Dubon O D, Sirmain G, Bründermann E, Hansen W L, Chamberlin D R, Linhart A M, Röser H P and Haller E E 1997 *Phys. Rev. B* **56** 12069
- [51] Altukhov I V, Kagan M S and Sinis V P 1988 *JETP Lett.* **47** 164
- [52] Altukhov I V, Kagan M S, Korolev K A, Sinis V P, Chirkova E G, Odnoblyudov M A and Yassievich I N 1989 *J. Exp. Theor. Phys.* **88** 51
- [53] Gousev Yu P, Altukhov I V, Korolev K A, Sinis V P, Kagan M S, Haller E E, Odnoblyudov M A, Yassievich I N and Chao K-A 1999 *Appl. Phys. Lett.* **75** 757
- [54] Altukhov I V, Kagan M S, Korolev K A, Sinis V P, Chirkova E G, Odnoblyudov M A and Yassievich I N 1999 *J. Exp. Theor. Phys.* **88** 51
- [55] Odnoblyudov M A, Yassievich I N, Kagan M S and Chao K A 2000 *Phys. Rev. B* **62** 15291
- [56] Ramdas A K and Rodriguez S 1981 *Rep. Prog. Phys.* **44** 80
- [57] Shastin V N 1996 *Proc. 21th Int. Conf. on Infrared and Millimeter Waves (Berlin)* ed M von Ortenberg and H-U Müller CT2 Orlova E E and Shastin V N 1996 *Ibid* p CTh4
- [58] Orlova E E, Zhukavin R Kh, Pavlov S G and Shastin V N 1988 *Phys. Status Solidi b* **210** 859

- [59] Shastin V N, Zhukavin R Kh, Orlova E E, Pavlov S G, Rümmeli M H, Hübers H-W, Hovenier J N, Klaassen T O, Riemann H, Bradley I V and van der Meer A F G 2002 *Appl. Phys. Lett.* **80** 3512
- [60] Lax M 1960 *Phys. Rev.* **119** 1502
- [61] Ascarelly G and Rodriguez S 1961 *Phys. Rev.* **124** 1321
- [62] Castner T G Jr 1963 *Phys. Rev.* **130** 58
- [63] Orlova E E 2002 *Proc. 26th Int. Conf. on the Physics of Semiconductors (Edinburgh)* p 61
- [64] Hübers H-W, Auen K, Pavlov S G, Orlova E E, Zhukavin R Kh and Shastin V N 1999 *Appl. Phys. Lett.* **74** 2655
- [65] Hübers H-W, Pavlov S G, Rümmeli M H, Zhukavin R Kh, Orlova E E, Andreev B A, Riemann H and Shastin V N *Physica B* **308–310** 232
- [66] Mayur A J, Sciacca M D, Ramdas A K and Rodriguez S 1993 *Phys. Rev. B* **48** 10893
- [67] Griffin A and Carruthers P 1963 *Phys. Rev.* **131** 1976
- [68] Hübers H-W, Pavlov S G, Greiner-Bär M, Rümmeli M H, Kimmitt M F, Zhukavin R Kh, Riemann H and Shastin V N 2002 *Phys. Status Solidi b* **233** 191
- [69] Pavlov S G, Hübers H-W, Orlova E E, Zhukavin R Kh, Riemann H, Nakata H and Shastin V N 2003 *Phys. Status Solidi b* **235** 126
- [70] Pavlov S G, Hübers H-W, Riemann H, Zhukavin R Kh, Orlova E E and Shastin V N 2002 *J. Appl. Phys.* **92** 5632
- [71] Onton A, Fisher P and Ramdas A K 1967 *Phys. Rev. Lett.* **19** 780
- [72] Asche M and Sarbei O G 1981 *Phys. Status Solidi b* **103** 11
- [73] Pavlov S G, Hübers H-W, Rümmeli M H, Zhukavin R Kh, Orlova E E, Shastin V N and Riemann H 2002 *Appl. Phys. Lett.* **80** 4717
- [74] Hübers H-W, Pavlov S G, Zhukavin R Kh, Riemann H, Abrosimov N V and Shastin V N 2004 *Appl. Phys. Lett.* **84** 3600
- [75] Zhukavin R, Pavlov S G, Kovalevsky K A, Hübers H-W, Riemann H and Shastin V N 2005 *J. Appl. Phys.* at press
- [76] Gershenson E M, Mel'nikov A P and Rabinovich R I 1985 *Electron–Electron Interactions in Disordered Systems* ed A L Efros and M Pollak (Amsterdam: Elsevier) p 483
- [77] Pavlov S G, Hübers H-W, Zhukavin R Kh, Riemann H and Shastin V N 2002 *Proc. 10th Int. Conf. on Terahertz Electronics (Cambridge, UK)* ed J M Chamberlain *et al* (Piscataway: IEEE, Inc.) p 93
- [78] Zwerdling S, Button K J and Lax B 1960 *Phys. Rev.* **118** 975
- [79] Aggarwal R L and Ramdas A K 1965 *Phys. Rev. A* **137** 602
- [80] Zhukavin R Kh *et al* 2003 *Appl. Phys. B* **76** 613
- [81] Andronov A A, Kozlov V A, Mazov L S and Shastin V N 1979 *JETP Lett.* **30** 551
- [82] Andronov A A, Mazov L S and Nefedov I M 1986 *Submillimeter Wave Lasers in Semiconductors using Hot Holes* ed A A Andronov (Gorki: Institute of Applied Physics) chapter 3, p 153
- [83] Starikov E V and Shiktorov P N 1991 *Opt. Quantum Electron.* **23** S177
- [84] Bründermann E, Haller E E and Muravjov A V 1998 *Appl. Phys. Lett.* **73** 723
- [85] Muravjov A V, Strijbos R C, Wenckebach W Th and Shastin V N 1998 *Phys. Status Solidi b* **205** 575
- [86] Adam T N, Troeger R T, Ray S K, Lv P-C and Kolodzey J 2003 *Appl. Phys. Lett.* **83** 1713
- [87] Lv P-C, Troeger R T, Adam T N, Kim S, Kolodzey J, Yassievich I N, Odnoblyudov M A and Kagan M S 2004 *Appl. Phys. Lett.* **85** 22–4
- [88] Dehlinger G, Diehl L, Gennser U, Sigg H, Faist J, Ensslin K, Grützmacher D and Müller E 2000 *Science* **290** 2277
- [89] Bates R *et al* 2003 *Appl. Phys. Lett.* **83** 4092
- [90] Murzyn P *et al* 2002 *Appl. Phys. Lett.* **80** 1456
- [91] Lynch S A *et al* 2002 *Mater. Sci. Eng. B* **89** 10
- [92] Altukhov I V, Chirkova E G, Sinis V P, Kagan M S, Gousev Yu P, Thomas S G, Wang K L, Odnoblyudov M A and Yassievich I N 2001 *Appl. Phys. Lett.* **79** 3909